Engineering Structures 32 (2010) 1199–1214

Contents lists available at ScienceDirect

Engineering Structures

journal homepage: www.elsevier.com/locate/engstruct

An efficient mathematical programming method for the elastoplastic analysis of frames

Konstantinos V. Spiliopoulos *, Theodoros N. Patsios

Institute of Structural Analysis & Antiseismic Research, Department of Civil Engineering, National Technical University of Athens, Zografou Campus, Zografos 157-80, Athens, Greece

ARTICLE INFO

Article history:
Received 17 August 2009
Received in revised form
12 December 2009
Accepted 22 December 2009
Available online 26 March 2010

Keywords:
Numerical methods
Quadratic programming
Force method
Graph theory
Plastic hinge
Plane bending
Moment/axial force interaction
Limit analysis
Pushover analysis
Cyclic loading

ABSTRACT

The elastoplastic nonholonomic analysis of frames is a nonlinear procedure in which the magnitude of the structural loading is incrementally modified using a proportional load factor, in accordance with a certain sequence of predefined loading patterns. It is an attempt by the structural engineering profession to estimate the strength as well as the deformations of framed structures under a given loading. In this work an analysis based on the force method and mathematical programming is presented. An elastic –perfectly plastic material is assumed and conventional plastic hinges of zero length are used to model the plasticity effects. The basis of the approach is the formulation of the incremental problem as a convex parametric quadratic programming (PQP) problem between two successive plastic hinges. A novel numerical strategy is proposed that uses a fictitious load factor to convert the PQP problem to a QP one. The solution of the QP problem, by an effective standard algorithm, establishes a feasible direction on which the true solution lies. The real solution is then found, simply on the demand of the formation of a new plastic hinge that is closest to open. Possible plastic unstressing is automatically accounted for. The approach is first developed for pure bending behaviour and is then extended to cater for moment/axial force interaction. Examples of application under monotonic, variable, and cyclic loading conditions are included. The whole procedure appears to be stable, robust, and computationally efficient as it requires much less time than the alternative displacement based direct stiffness method.

1. Introduction

Elastoplastic analysis is an important procedure to determine the capacity of a structure beyond its elastic limits. In the course of this analysis, the external loads are continuously applied with more and more structural components yielding. A series of elastic analyses are therefore generated by modifying the mathematical model of the structure to account for reduced resistance of yielding components. The procedure consists of the superposition of these analyses and stops when the structure cannot carry any further load and becomes unstable, or until a predetermined load limit is reached. Thus a good estimate of the strength of the structure as well as of its ductility can be made.

In an early work, Maier [1] has shown that quadratic programming (QP) provides a unified theoretical framework for the elastoplastic analysis of frames. In the context of holonomic plasticity various QPs for total quantities are written down taking into account perfectly plastic, work-hardening or even softening behaviour. An incremental form of a QP in terms of kinematic variables also appears in the same work. Duality QPs are presented in a subsequent paper [2]. The formulation of the problem as a parametric linear complementarity problem (PLCP) has been given by Maier [3]. Linear programming (LP) is the main ingredient to solve such problems and a numerical solution based on the Simplex method has appeared in De Donato and Maier [4] together with some examples and an extension to include non-proportional loading.

Smith [5] and Maier et al. [6], almost at the same time, proposed numerical solutions of the PLCP problem based on the Simplex method and enforcing complementarity at each pivotal step, thus, restricting the variables to enter the basis. With slight modifications of the algorithms, they managed to extend the solutions to the case of nonholonomic plasticity. Extension to piecewise proportional loading is also reported in [6].

In an attempt to provide general purpose computer programs Franchi and Cohn [7] produced a rather involved PLCP based algorithm and applied it to a single storey plane frame. Kaneko [8] used the same formulation but worked directly on incremental quantities and was able to assess nonholonomic plasticity without having to make any computational adjustments (as in [5,6]). Wakefield and Tin-Loi [9] applied this method to grillages and multi-storey frames. Formulations based on PLCP have also recently been employed by Cocchetti and Maier [10] and Tangaramvong and Tin-Loi [11,12] to account for local softening behaviour.

* Corresponding author. Tel.: +30 210 7721603; fax: +30 210 7721604.
E-mail address: kvspilio@central.ntua.gr (K.V. Spiliopoulos).

0141-0296/$ – see front matter © 2009 Elsevier Ltd. All rights reserved.
doi:10.1016/j.engstruct.2009.12.045

All the aforementioned procedures for the elastoplastic analysis of frames are based on mathematical programming (MP). One should only note here, that in the context of the evaluation of the limit load of frames only, Marin-Artieda and Dargush [13] have presented an approach that uses the Linear Matching method, which is not formulated within MP but appears to have difficult convergence properties. A more thorough presentation of the approach together with improved convergence appeared quite recently in Barrera et al. [14].

Although MP provides an ideal mathematical framework for encoding the basic theory of elastic–plastic structures, the solutions schemes referred to, as above, generally involve large number of variables and constraints (Tin-Loi and Wong [15]). For this reason the, displacement based, direct stiffness method has been used almost exclusively and all commercial programs are based on it (e.g. SAP2000 [16]). Following this method, an event-to-event strategy is employed which takes into account the reduction of the resistance whenever a plastic hinge occurs or the increase in the resistance of a plastic hinge whenever local unloading occurs by re-formulating and re-decomposing the stiffness matrix.

The main issue in the elastoplastic analysis of frames is the requirement of a statically admissible and safe distribution of stresses throughout the whole structure. The most natural formulation therefore appears to be within the framework of the force method of analysis, since equilibrium may be expressed accurately as a linear combination of the hyperstatic forces and the applied loading. On the contrary, if one uses the displacement method of analysis, a degree of approximation is needed (Pereira et al. [17]). Nevertheless, the displacement method has been almost exclusively in use, because it is easier to automate.

The main problem with the force method towards this automation is the way to pre-select the hyper-static forces, which are the main unknowns. Approaches to deal with this problem are to set up a displacement method based environment and transform it to a force method based one, using algebraic methods (Damkilde and Høyer [18]). This transformation, of course, involves a degree of approximation.

It has been realized, quite early (e.g. Spillers [19]), that graph theory and the graph representation of a frame may provide a direct way to automate the force method. It may be proved that, for a 'planar graph' there is a unique number of closed loops called cycle basis. Spiliopoulos [20] has proposed a relatively easily programmable algorithm which constructs such a basis using a minimum path technique between two nodes of a graph. This algorithm has been used together with LP for the optimum plastic design of frames under monotonic or variable loading (Spiliopoulos [20,21]).

In this work, the numerical solution of the small displacement elastoplastic analysis of frames, using the force method is presented. The material is considered elastic rigid-plastic with nonholonomic behaviour, whereas the adopted model is a plastic hinge model of zero length. The basis of the formulation consists in decomposing the increments of the stress resultants in two terms, one due to the indeterminacy of the structure and one due to the increments of the load. The problem is cast, not as the solution of a PLCP, but as a direct solution of the parametric quadratic program (PQP) at the beginning of each incremental loading step, the parameter being the incremental load factor. A novel numerical strategy is proposed which, by employing a fictitious load factor, converts the solution of this PQP to the solution of a simple QP. This QP may be solved using standard algorithms (e.g. Goldfarb and Idnani [22]). Possible plastic unstressing, in a stepwise-holonomic fashion, is automatically detected by the solution of the fictitious problem. One may, thus, predetermine the direction on which the real solution of the current incremental step lies. This solution is then found merely on the demand that a new plastic hinge forms.

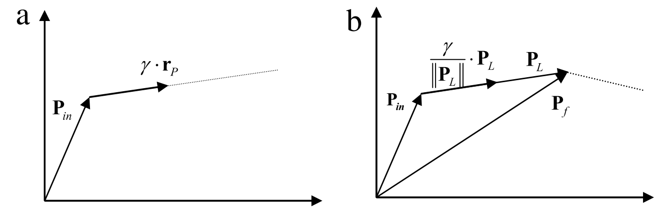

Fig. 1. Proportional loading: (a) limit load analysis, (b) prescribed loading analysis.

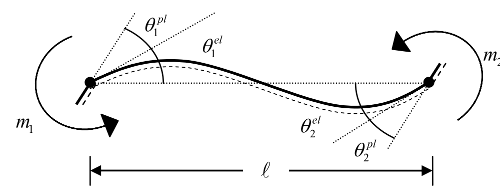

Fig. 2. Rotations and moments at member's ends.

The procedure is formulated with respect to proportional or piecewise proportional loading. Since bending is the prevailing mode of deformation for framed structures, in the Sections 2–4 of the present paper, the procedure is developed under the assumption of a pure bending behaviour. The essential features of the method are also discussed in these sections. In Section 5 the procedure is extended to include also the effects of the axial force. Examples of application appear in Section 6 that indicate the effectiveness of the method for either monotonic loading, loading scenarios or cyclic loading. The computational efficiency of the procedure compared to the direct stiffness method is also demonstrated.

2. Governing equations for pure bending

Let us suppose that a frame, whose material behaves as elastic–perfectly plastic, is subjected to a proportionally changing loading pattern of the form

$$\mathbf{P} = \mathbf{P}_{in} + \gamma \cdot \mathbf{r}_P \tag{1}$$

where, using bold letters to represent vectors and matrices throughout, $\mathbf{P}_{in}$ is an initial loading state, γ is a proportional loading parameter which controls the further application of loading, $\mathbf{r}_P$ is the unit vector along the direction of the loading pattern (Fig. 1). Either for the case of a limit analysis or a prescribed loading analysis, $\mathbf{r}_P$ may be directly computed. In the prescribed loading case, for a particular branch, with initial and final loading states $\mathbf{P}_{in}$ and $\mathbf{P}_f$ respectively, $\mathbf{r}_P = (1/\|\mathbf{P}_L\|) \cdot \mathbf{P}_L$, where $\mathbf{P}_L = \mathbf{P}_f - \mathbf{P}_{in}$ (Fig. 1(b)).

In response to the external loading, every member of the structure, which is defined as a line/curve lying between two nodes, develops two rotations at its ends, relatively to a local axis defined by its chord; these rotations may be decomposed into an elastic and a plastic component (plastic hinge approach) (Fig. 2).

One may write the elastic rotations in terms of the end moments using the member's flexibility matrix:

$$\begin{Bmatrix} \theta_1^{el} \\ \theta_2^{el} \end{Bmatrix} = \frac{\ell}{6EI} \cdot \begin{bmatrix} 2 & 1 \\ 1 & 2 \end{bmatrix} \cdot \begin{Bmatrix} m_1 \\ m_2 \end{Bmatrix} \tag{2}$$

where ℓ and EI are the member's length and bending stiffness.

By grouping all the individual flexibility matrices of the structure in a block-diagonal matrix $\mathbf{F}_m$, one may write for all the elastic rotations and the end moments of the frame:

$$\boldsymbol{\theta}^{el} = \mathbf{F}_m \cdot \mathbf{m}. \tag{3}$$

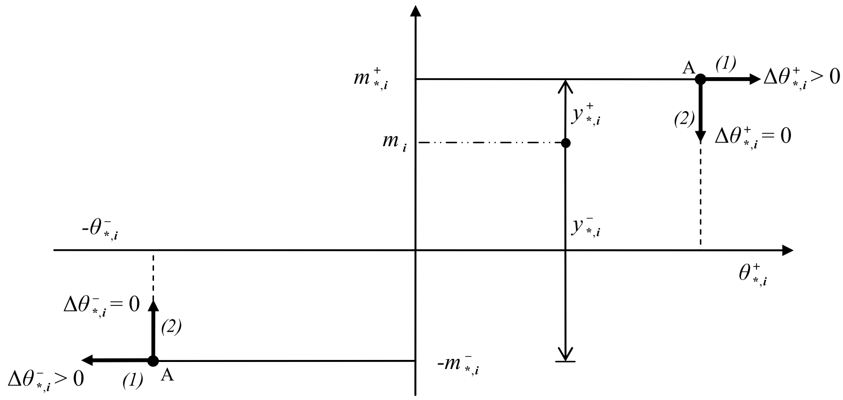

Fig. 3. Rigid-plastic behaviour and plastic unstressing.

Due to the nonlinear (elastoplastic) behaviour, the solution will be acquired in incremental steps. At the end of such a step, an increment of the applied loading will create an increment of moments which may be determined, using the force (or mesh) description:

$$\Delta\mathbf{m} = \mathbf{B}_m \cdot \Delta\mathbf{p} + \Delta\gamma \cdot \mathbf{B}_{o,m} \cdot \mathbf{r}_P. \tag{4}$$

The first term is due to the indeterminacy of the structure with $\mathbf{p}$ being a set of hyperstatic forces, called a statical basis. These forces may be introduced in the structure by making cuts at each closed loop of the indeterminate frame and converting it to a determinate one. The second term is due to the equilibrium with the increment of the applied loads expressed through the increment $\Delta\gamma$ of the proportional load factor.

The increments of the total rotations will then be given by:

$$\Delta\boldsymbol{\psi} = \Delta\boldsymbol{\theta}^{el} + \Delta\boldsymbol{\theta}^{pl}. \tag{5}$$

From the principle of static kinematic duality (SKD), the conjugate to the hyperstatic forces discontinuities at the cuts are related to the above increments of rotations through the matrix $\mathbf{B}_m^T$. Closing these cuts provides us with the conditions of compatibility, as was first proposed by Maxwell:

$$\mathbf{B}_m^T \cdot \Delta\boldsymbol{\psi} = \mathbf{0}. \tag{6}$$

Eq. (3) may be used to compute $\Delta\boldsymbol{\theta}^{el}$. By combining (4) and (5), Eq. (6) becomes:

$$\mathbf{B}_m^T \cdot \mathbf{F}_m \cdot \left[\mathbf{B}_m \cdot \Delta\mathbf{p} + \Delta\gamma \cdot \mathbf{B}_{0,m} \cdot \mathbf{r}_P\right] + \mathbf{B}_m^T \cdot \Delta\boldsymbol{\theta}^{pl} = \mathbf{0}. \tag{7}$$

Depending on whether the bending moment that has reached the plastic capacity m_* of a cross section causes tension or compression at the bottom side of a cross-section (pre-selected "positive" fiber, Fig. 2) we may have positive or negative plastic rotations with reference to the local coordinate system of the member, respectively. So, in general, one may write:

$$\Delta\boldsymbol{\theta}^{pl} = \Delta\boldsymbol{\theta}_*^+ - \Delta\boldsymbol{\theta}_*^- = \left[\mathbf{I} \;\vdots\; -\mathbf{I}\right] \cdot \begin{Bmatrix} \Delta\boldsymbol{\theta}_*^+ \\ \Delta\boldsymbol{\theta}_*^- \end{Bmatrix} = \mathbf{N} \cdot \Delta\boldsymbol{\theta}_* \tag{8}$$

where $\Delta\boldsymbol{\theta}_*^+$ and $\Delta\boldsymbol{\theta}_*^-$ are positive numbers and constitute the elements of $\Delta\boldsymbol{\theta}_*$.

Assuming rigid plastic behaviour, the relationship between a bending moment and its corresponding plastic rotation, whether we have further loading, or plastic unstressing (nonholonomic behaviour), may be seen in Fig. 3, and may be expressed by a single equation (complementarity relation) as follows:

$$\mathbf{y}^T \cdot \Delta\boldsymbol{\theta}_* = 0 \quad \text{where } \mathbf{y} \geq \mathbf{0},\ \Delta\boldsymbol{\theta}_* \geq \mathbf{0} \tag{9}$$

where $\mathbf{y}_* = \begin{Bmatrix} \mathbf{y}_*^+ \\ \mathbf{y}_*^- \end{Bmatrix}$ collects the plastic potentials at every cross section that are defined in Fig. 3.

If we denote by $\mathbf{m}_{k-1}$ the moments of the previously converged incremental step, the non-negativity of the plastic potentials makes possible to express the static admissibility condition of the bending moments at the current incremental step k as:

$$\mathbf{y}_* + \mathbf{N}^T \cdot (\Delta\mathbf{m} + \mathbf{m}_{k-1}) = \mathbf{m}_* \tag{10}$$

where $\mathbf{m}_* = \begin{Bmatrix} \mathbf{m}_*^+ \\ \mathbf{m}_*^- \end{Bmatrix}$ collects the plastic capacities of the cross sections in positive and negative bending, respectively (Fig. 3).

Eqs. (7)–(10), combined with (4), may serve as the Karush–Kuhn–Tucker relations that lead to the solution of the following quadratic program (QP) at every incremental step k:

$$\begin{aligned} \text{Minimize } z(\Delta\mathbf{p}) \;=\; & \frac{1}{2} \cdot \Delta\mathbf{p}^T \cdot (\mathbf{B}_m^T \cdot \mathbf{F}_m \cdot \mathbf{B}_m) \cdot \Delta\mathbf{p} \\ & + \Delta\gamma_k \cdot (\mathbf{B}_m^T \cdot \mathbf{F}_m \cdot \mathbf{B}_{o,m} \cdot \mathbf{r}_P)^T \cdot \Delta\mathbf{p} \\ \text{Subject to: } & (\mathbf{N}^T \cdot \mathbf{B}_m) \cdot \Delta\mathbf{p} \leq (\mathbf{m}_* - \mathbf{N}^T \cdot \mathbf{m}_{k-1}) - \Delta\gamma_k \cdot (\mathbf{N}^T \cdot \mathbf{B}_{o,m} \cdot \mathbf{r}_P) \end{aligned} \tag{11}$$

with $\Delta\gamma_k$ being the increment of the load factor at the current step.

It appears that a more accurate numerical solution may be achieved if each constraint is divided by its corresponding plastic capacity so that the right-hand side of (10) is equal to one. So the QP to be solved is:

$$\begin{aligned} \text{Minimize } z(\Delta\mathbf{p}) \;=\; & \frac{1}{2} \cdot \Delta\mathbf{p}^T \cdot \left(\mathbf{B}_m^T \cdot \mathbf{F}_m \cdot \mathbf{B}_m\right) \cdot \Delta\mathbf{p} \\ & + \Delta\gamma_k \cdot (\mathbf{B}_m^T \cdot \mathbf{F}_m \cdot \mathbf{B}_{o,m} \cdot \mathbf{r}_P)^T \cdot \Delta\mathbf{p} \\ \text{Subject to: } & (\mathbf{M}_*^T \cdot \mathbf{B}_m) \cdot \Delta\mathbf{p} \leq \mathbf{e} - \mathbf{M}_*^T \cdot \mathbf{m}_{k-1} - \Delta\gamma_k \cdot (\mathbf{M}_*^T \cdot \mathbf{B}_{o,m} \cdot \mathbf{r}_P) \end{aligned} \tag{12}$$

where

$$\mathbf{M}_* = \left[\begin{array}{ccc|ccc} 1/m^+_{*,1} & & & -1/m^-_{*,1} & & \\ & \ddots & & & \ddots & \\ & & 1/m^+_{*,N_c} & & & -1/m^-_{*,N_c} \end{array}\right] = \left[\left[diag(\mathbf{m}_*^+)\right]^{-1} \;\vdots\; \left[-diag(\mathbf{m}_*^-)\right]^{-1}\right]$$

with N_c being the total number of critical sections. The product $\mathbf{B}_m^T \cdot \mathbf{F}_m \cdot \mathbf{B}_m$ is the flexibility matrix of the structure for the selected set of the hyperstatic forces, and $\mathbf{e}^T = \{1\ 1\ \cdots\ 1\}$ is a column vector.

The way to solve this QP problem will be discussed in Section 4. Here, we should note that, the product of the Lagrange multipliers of the optimal solution with $\mathbf{M}_*$ provides the increments of the plastic rotations, $\Delta\boldsymbol{\theta}_*$.

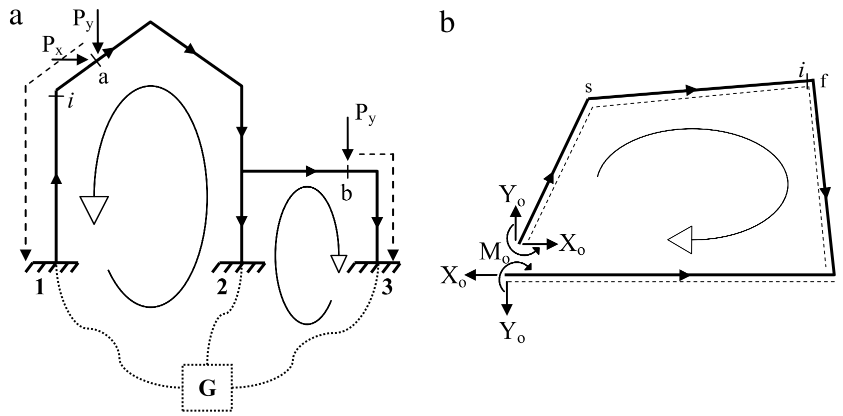

Fig. 4. (a) Typical cycle basis and shortest path cantilevers, (b) Self equilibrating system of forces.

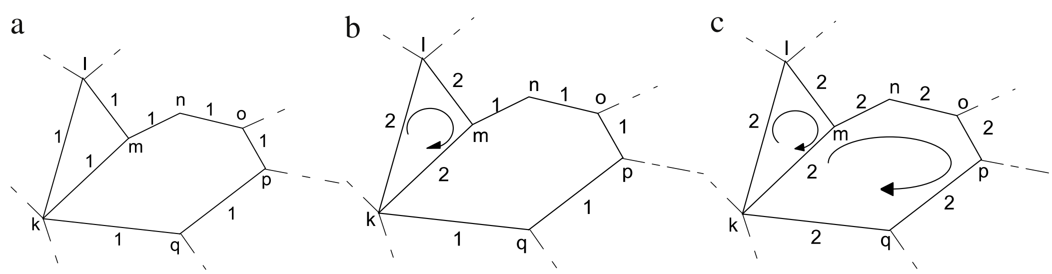

Fig. 5. Mesh base formation.

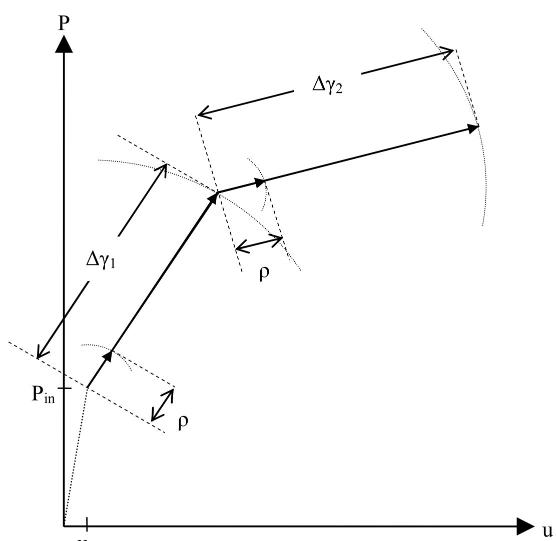

Fig. 6. Fictitious (ρ), and true incremental load factors ($\Delta\gamma$).

3. Selection of the hyperstatic forces

The automation of the process depends on the selection of the hyperstatic forces which is called statical basis. An algorithm has been published (Spiliopoulos [20], where more details may be found), which finds such a basis by selecting a set of independent cycles which is equal to Betti's number for planar graphs. Each frame is such a graph (Fig. 4(a)) and Betti's number is equal to $\mu - \nu + 1$ where μ, ν are the number of members and nodes that compose the graph. The ground is represented by an extra node and extra members are used to connect this node to each foundation node.

This algorithm is easy to implement because it is based on initially setting the lengths of each member (not in the Euclidean sense) equal to 1. The procedure then starts from the node that has the maximum number of members incident to it, finds the minimum path between the ends of each of the members, not by going along the member but going around it. The minimum path together with the generator member forms a cycle candidate to enter the mesh basis. It will enter the mesh basis if the following admissibility rule is satisfied:

"The length of the path is less that 2*(*nodes along the path*-1)".

If this rule is satisfied the cycle enters the basis and all the members of this cycle get the length of 2.

As an example of a cycle basis formation, the procedure that was just described is used to establish a cycle basis in the sub graph (Fig. 5(a)) that has been extracted from a main graph. Starting from node k, the cycle *klmk* is selected (Fig. 5(b)) using *km* as a generator member and all the lengths of the members of the cycle take the value of 2. There is no way of re-entry in the basis of this cycle, since the admissibility rule is not satisfied. By picking up a next member, e.g. (*mn*), a next cycle may be selected to enter the basis (Fig. 5(c)). There are cases of complicated graphs that this simple process may break down, but there are remedies to overcome this problem [20].

By making a cut at each cycle, one may establish a pair of two unknown forces X_o, Y_o along the x and y directions and an unknown bending moment M_o at the point of the cut, with coordinates x_o and y_o. These are the three indeterminate entities for the cycle at hand (Fig. 4(b)). The bending moment at any cross section i along the cycle with coordinates x_i and y_i, are given by:

$$m_i = (\pm)\left[(y_o - y_i) \quad (x_i - x_o) \quad -1\right] \cdot \begin{Bmatrix} X_o \\ Y_o \\ M_o \end{Bmatrix} \tag{13}$$

where the positive or the negative sign depends on whether the mesh orientation coincides with the member orientation, that the cross section belongs to, or not. By filling in the appropriate positions the matrix $\mathbf{B}_m$ may be formed.

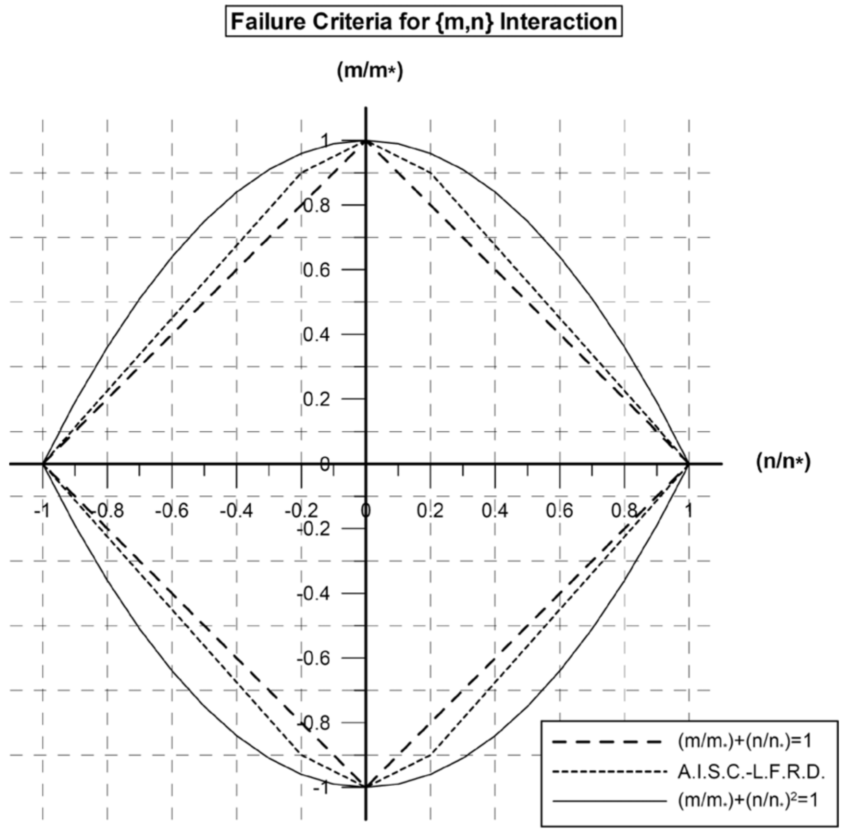

Fig. 7. Various types of failure criteria considering bending moment & axial force interaction.

3.1. Equilibrium with external forces

Equilibrium with the applied loading is accomplished through the use of cantilevers, which mark the quickest way to the ground of the points of application of the loads (Fig. 4(a)). For a cross section i located along this way, the bending moment m is given by:

$$m_i = (\pm)\left[(y_a - y_i) \quad (x_a - x_i)\right] \cdot \begin{Bmatrix} P_x \\ P_y \end{Bmatrix} \tag{14}$$

with x_a and y_a the coordinates of the point where the concentrated loads are applied.

The positive sign in the parenthesis is valid if the orientations of the member that this section belongs to, and the direction of the cantilever, coincide.

Using (14) for all the critical sections and all the loads, the matrix $\mathbf{B}_{o,m}$ may be constructed.

Distributed loading of a member may be approximated by splitting it into a set of finite elements of equal length, and applying statically equivalent point loads at their nodes. For a more precise implementation of the distributed loading, one may include an additional term in Eq. (3) that corresponds to the free elastic rotations (see for example, [5]).

4. Proposed numerical strategy

The QP problem (12) is a parametric one, since, although the basic unknowns are the hyperstatic forces $\Delta\mathbf{p}$, the parameter $\Delta\gamma_k$ should also be supplied. This parameter may be estimated requiring that each load increment ends with the formation of a new plastic hinge.

In this work, a novel numerical strategy to solve directly the QP problem (12) is suggested. Starting with an initial value of $\gamma = 0$ and $k = 1$, the following steps describe this strategy:

1. Adopt a "fictitious" small initial value for $\Delta\gamma_k = \rho$.
2. Solve the QP problem (12) and obtain a "fictitious" set of increments of hyperstatic forces $\Delta\tilde{\mathbf{p}}$ and, using the Lagrange multipliers of the optimal solution, a set of "fictitious" increments of plastic rotations $\Delta\tilde{\boldsymbol{\theta}}_*$. The QP algorithm [22] is used.
3. Normalize the increments of the "fictitious" set of hyperstatic forces and plastic rotations:

$$\Delta\mathbf{p}' = \frac{1}{\rho} \cdot \Delta\tilde{\mathbf{p}} \quad \text{and} \quad \Delta\boldsymbol{\theta}'_* = \frac{1}{\rho} \cdot \Delta\tilde{\boldsymbol{\theta}}_*. \tag{15}$$

4. Evaluate the corresponding incremental bending moment diagram using (4), normalized with respect to "ρ":

$$\Delta\mathbf{m}' = \mathbf{B}_m \cdot \Delta\mathbf{p}' + \mathbf{B}_{o,m} \cdot \mathbf{r}_P. \tag{16}$$

5. Find the correct $\Delta\gamma_k$ as the minimum $\Delta\gamma_{i,k}$ that produces a new either positive or negative plasticization of a critical cross section i:

$$m_{i,k-1} + (\Delta\gamma_{i,k}) \cdot \Delta m'_i = m^+_{*,i} \quad \text{or}$$
$$m_{i,k-1} + (\Delta\gamma_{i,k}) \cdot \Delta m'_i = -m^-_{*,i} \tag{17}$$

for $i = 1, 2, \ldots, N_c$, where N_c is the total number of critical sections
6. Find the increments of the bending moments and the plastic rotations:

$$\Delta\mathbf{m} = \Delta\gamma_k \cdot \Delta\mathbf{m}' \quad \text{and} \quad \Delta\boldsymbol{\theta}_* = \Delta\gamma_k \cdot \Delta\boldsymbol{\theta}'_*. \tag{18}$$

7. Update the load factor and the various static and kinematic variables:

$$\begin{aligned} &\gamma_k = \gamma_{k-1} + \Delta\gamma_k \\ &\mathbf{m}_k = \mathbf{m}_{k-1} + \Delta\mathbf{m} \\ &\boldsymbol{\theta}^{el}_k = \mathbf{F}_m \cdot \mathbf{m}_k \\ &\boldsymbol{\theta}^{pl}_k = \boldsymbol{\theta}^{pl}_{k-1} + \Delta\boldsymbol{\theta}^{pl} \\ &\boldsymbol{\psi}_k = \boldsymbol{\theta}^{el}_k + \boldsymbol{\theta}^{pl}_k \end{aligned} \tag{19}$$

where use of (8) is made.

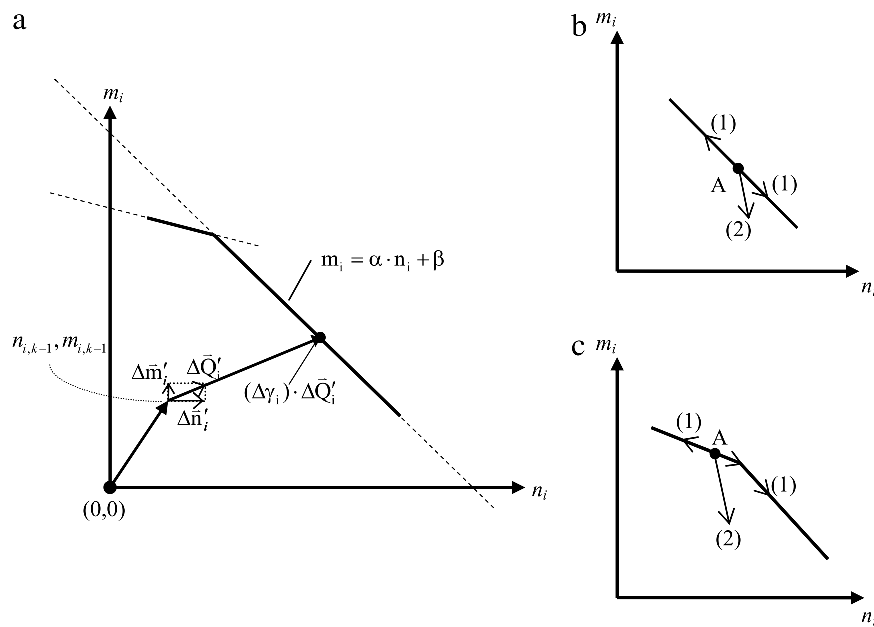

Fig. 8. (a) Search direction for plasticization from elastic state (b), (c) Further plasticization (1) or unloading (2).

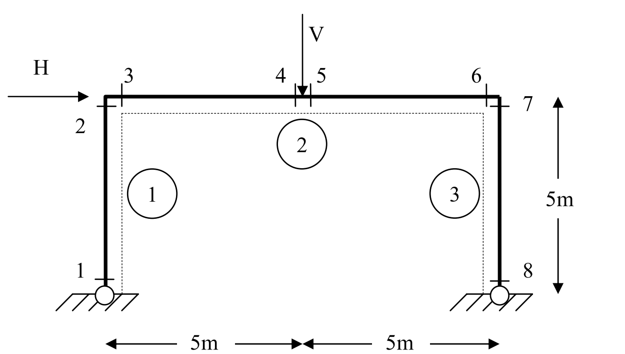

Member	EI (kNm^2)	M_p (kNm)
1	10000.0	100.0
2	10000.0	350.0
3	10000.0	200.0

Fig. 9. Frame's geometry, mechanical properties, loading, and critical section numbering.

The displacements at the loaded points may be found using SKD between rotations and displacements:

$$\mathbf{u}_k = \mathbf{B}_{o,m}^T \cdot \boldsymbol{\psi}_k. \tag{20}$$

8. Return to step 1 and repeat the process for $k = k + 1$, until either
   (a) no solution of the QP may be found, meaning a collapse state has been reached and γ_k is the limit load factor, *or*
   (b) if we have a prescribed loading case and (a) has not occurred, the process stops if $|\gamma_k - \|P_L\|| \le \rho$, meaning we have reached the end of the current branch.

The algorithm automatically detects whether at the beginning of the incremental step we have further plasticization of an already plasticized critical section (point A, Fig. 3, movement along the direction (1) on the yield plane) or local unloading (direction (2)). This is determined from the value of the corresponding Lagrange multiplier, which is readily available after the solution of the "fictitious" QP problem: in the case where this value is positive we have further loading, or if the value is zero we have plastic unstressing.

A physical explanation on the use of a "fictitious" starting load factor is that it enables one to establish a feasible direction on which the incremental step lies, whose true length is then found on the grounds of the formation of a new plastic hinge. The procedure may be pictured for two steps on a force–displacement diagram (Fig. 6).

5. Extension to bending moment and axial force interaction

The method presented above may be extended to cases with stress resultant interactions, the commonest of which is between bending moments and axial forces.

For fully plasticized orthogonal steel sections, this interaction is generally known to be represented by the symmetric, quadratic and convex curve given by the following equation:

$$\frac{|m|}{m_*} + \left(\frac{n}{n_*}\right)^2 = 1 \tag{21}$$

where m_* and n_* represent the section's bending moment and axial force bearing capacities.

The above yield curve may be approximated by a finite set of "ζ" independent linear equations for each of the four quadrants:

$$f(m,n) = (\pm)s_1 \cdot \frac{m}{m_*} + (\pm)\,s_2 \cdot \frac{n}{n_*} - 1 = 0 \tag{22}$$

with the positive or negative signs in the parentheses depending on the particular quadrant.

We have "ζ" distinct couples of (s_1, s_2).

The simplest linearization ($\zeta = 1$), consists of the four lines shown dashed in Fig. 7. For the AISC LRFD criterion [23], on the other hand, $\zeta = 2$.

Now, at every critical cross-section, one should supply, besides the bending moment, the axial force also. Eqs. (13) and (14) can be found to take the form:

$$\begin{Bmatrix} m_i \\ n_i \end{Bmatrix} = (\pm)\left[\begin{array}{c:c:c} (y_o - y_i) & (x_i - x_o) & -1 \\ \hdashline -\cos\varphi & -\sin\varphi & 0 \end{array}\right] \cdot \begin{Bmatrix} X_o \\ Y_o \\ M_o \end{Bmatrix} \tag{23}$$

$$\begin{Bmatrix} m_i \\ n_i \end{Bmatrix} = (\pm)\left[\begin{array}{c:c} (y_a - y_i) & (x_a - x_i) \\ \hdashline \cos\varphi & -\sin\varphi \end{array}\right] \cdot \begin{Bmatrix} P_x \\ P_y \end{Bmatrix} \tag{24}$$

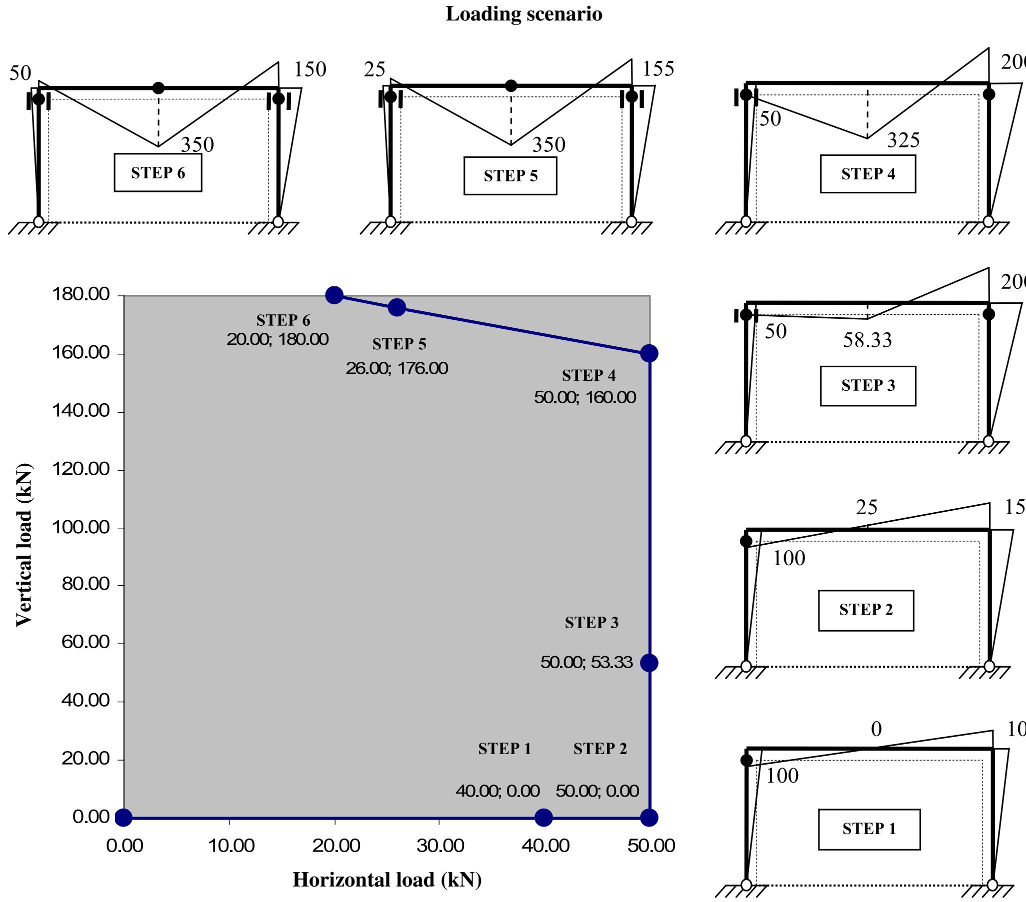

Fig. 10. Loading scenario's coordinates for each analysis step, plasticization/local unstressing sequence, quantitative bending moment diagrams (units: kN, m).

with

$$\cos\varphi = \frac{x_f - x_s}{\sqrt{(x_f - x_s)^2 + (y_f - y_s)^2}} \quad \text{and}$$

$$\sin\varphi = \frac{y_f - y_s}{\sqrt{(x_f - x_s)^2 + (y_f - y_s)^2}}$$

where (x_s, y_s) and (x_f, y_f) are the coordinates of the two ends of the member that the critical section i belongs to (Fig. 4(b)) and the positive signs hold under the same assumptions as in Section 3.

Elastic axial elongations will now appear besides the elastic rotations, so that (3) will now look like:

$$\mathbf{q}^{el} = \bar{\mathbf{F}} \cdot \mathbf{Q} \tag{25}$$

where

$$\mathbf{q}^{el} = \begin{Bmatrix} \boldsymbol{\theta}^{el} \\ \boldsymbol{\delta}^{el} \end{Bmatrix}, \quad \bar{\mathbf{F}} = \begin{bmatrix} \mathbf{F}_m & [\varnothing] \\ [\varnothing] & \mathbf{F}_n \end{bmatrix}, \quad \mathbf{Q} = \begin{Bmatrix} \mathbf{m} \\ \mathbf{n} \end{Bmatrix}$$

with $\mathbf{F}_n$ relating the elastic axial elongations at the two critical sections at the ends of the member with the corresponding axial forces, through its axial flexibility, ℓ/EA.

Collecting all the bending moments and axial forces of the critical sections in the matrices $\mathbf{m}$ and $\mathbf{n}$ we may write at the current incremental step k:

$$\mathbf{m}_k = \Delta\mathbf{m} + \mathbf{m}_{k-1} \quad \text{and} \quad \mathbf{n}_k = \Delta\mathbf{n} + \mathbf{n}_{k-1} \tag{26}$$

where $\Delta\mathbf{m}$ and $\Delta\mathbf{n}$ may be computed with the aid of Eqs. (23) and (24):

$$\begin{Bmatrix} \Delta\mathbf{m} = \mathbf{B}_m \cdot \Delta\mathbf{p} + (\Delta\gamma_k) \cdot \mathbf{B}_{o,m} \cdot \mathbf{r}_p \\ \Delta\mathbf{n} = \mathbf{B}_n \cdot \Delta\mathbf{p} + (\Delta\gamma_k) \cdot \mathbf{B}_{o,n} \cdot \mathbf{r}_p \end{Bmatrix}$$

$$\rightarrow \Delta\mathbf{Q} = \bar{\mathbf{B}} \cdot \Delta\mathbf{p} + \Delta\gamma_k \cdot \bar{\mathbf{B}}_o \cdot \mathbf{r}_p \tag{27}$$

where $\bar{\mathbf{B}} = \begin{bmatrix} \mathbf{B}_m \\ \mathbf{B}_n \end{bmatrix}, \quad \bar{\mathbf{B}}_o = \begin{bmatrix} \mathbf{B}_{o,m} \\ \mathbf{B}_{o,n} \end{bmatrix}$.

The generalized plastic displacement now at a critical section i consists of two components; a plastic rotation and an axial discontinuity, which may be computed with the help of (22):

$$\Delta\mathbf{q}_i^{pl} = \begin{Bmatrix} \Delta\theta_i^{pl} \\ \Delta\delta_i^{pl} \end{Bmatrix} = \Delta\lambda_i \cdot \frac{\partial f}{\partial \mathbf{Q}_i} = \Delta\lambda_i \cdot \begin{Bmatrix} s_1/m_{*i} \\ s_2/n_{*i} \end{Bmatrix}. \tag{28}$$

Collecting the plastic rotations at the top and the axial discontinuities at the bottom, of all the critical sections, one may form $\Delta\mathbf{q}^{pl} = \begin{Bmatrix} \Delta\boldsymbol{\theta}^{pl} \\ \Delta\boldsymbol{\delta}^{pl} \end{Bmatrix}$.

With complementarity now holding between $\Delta\lambda_i$ and the section's generalized plastic potential (distance from the yield surfaces of Eq. (22)), the QP program (Eq. (12)) may be written as:

$$\begin{aligned} \text{Minimize } z(\Delta\mathbf{p}) &= \frac{1}{2} \cdot \Delta\mathbf{p}^T \cdot (\bar{\mathbf{B}}^T \cdot \bar{\mathbf{F}} \cdot \bar{\mathbf{B}}) \cdot \Delta\mathbf{p} \\ &\quad + \Delta\gamma_k \cdot (\bar{\mathbf{B}}^T \cdot \bar{\mathbf{F}} \cdot \bar{\mathbf{B}}_o \cdot \mathbf{r}_p)^T \cdot \Delta\mathbf{p} \\ \text{Subject to: } & (\bar{\mathbf{N}}^T \cdot \bar{\mathbf{B}}) \cdot \Delta\mathbf{p} \le \mathbf{e} - \bar{\mathbf{N}}^T \cdot \mathbf{Q}_{k-1} - \Delta\gamma_k \cdot (\bar{\mathbf{N}}^T \cdot \bar{\mathbf{B}}_o \cdot \mathbf{r}_p) \end{aligned} \tag{29}$$

where "$\bar{\mathbf{N}}$" is a matrix that stores in the appropriate positions the various coefficients of the left-hand side of the constraints (Eq. (22)). Depending on the number of the linear segments of our yield criterion we may have "ζ" distinct couples of (s_1, s_2), i.e. $(s_1, s_2) = \{(s_{11}, s_{21}), (s_{12}, s_{22}), \ldots, (s_{1\zeta}, s_{2\zeta})\}$. Therefore see

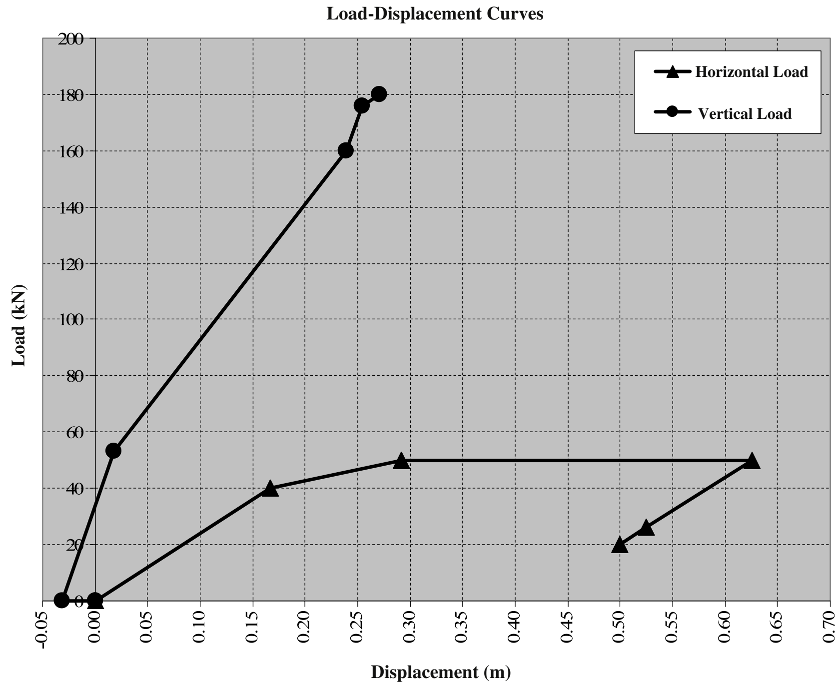

Fig. 11. Load vs. corresponding displacement curves.

$$\bar{\mathbf{N}} = \left[\; \overbrace{\left[\bar{\mathbf{N}}_{\mathrm{I}} \mid \bar{\mathbf{N}}_{\mathrm{II}} \mid \bar{\mathbf{N}}_{\mathrm{III}} \mid \bar{\mathbf{N}}_{\mathrm{IV}}\right]}^{(s_{11},s_{21})} \;\Big|\; \overbrace{\left[\bar{\mathbf{N}}_{\mathrm{I}} \mid \bar{\mathbf{N}}_{\mathrm{II}} \mid \bar{\mathbf{N}}_{\mathrm{III}} \mid \bar{\mathbf{N}}_{\mathrm{IV}}\right]}^{(s_{12},s_{22})} \;\Big|\; \ldots\ldots \;\Big|\; \overbrace{\left[\bar{\mathbf{N}}_{\mathrm{I}} \mid \bar{\mathbf{N}}_{\mathrm{II}} \mid \bar{\mathbf{N}}_{\mathrm{III}} \mid \bar{\mathbf{N}}_{\mathrm{IV}}\right]}^{(s_{1\zeta},s_{2\zeta})} \;\right]$$

Box I.

Box I, where:

$$\bar{\mathbf{N}}_{\mathrm{I}} = \left[\begin{array}{c:c} s_1 \cdot \left[diag(\mathbf{m}_*^+)\right]^{-1} & [\varnothing] \\ \hdashline [\varnothing] & s_2 \cdot \left[diag(\mathbf{n}_*^+)\right]^{-1} \end{array}\right],$$

$$\bar{\mathbf{N}}_{\mathrm{II}} = \left[\begin{array}{c:c} s_1 \cdot \left[diag(\mathbf{m}_*^+)\right]^{-1} & [\varnothing] \\ \hdashline [\varnothing] & s_2 \cdot \left[-diag(\mathbf{n}_*^-)\right]^{-1} \end{array}\right],$$

$$\bar{\mathbf{N}}_{\mathrm{III}} = \left[\begin{array}{c:c} s_1 \cdot \left[-diag(\mathbf{m}_*^-)\right]^{-1} & [\varnothing] \\ \hdashline [\varnothing] & s_2 \cdot \left[diag(\mathbf{n}_*^+)\right]^{-1} \end{array}\right],$$

$$\bar{\mathbf{N}}_{\mathrm{IV}} = \left[\begin{array}{c:c} s_1 \cdot \left[-diag(\mathbf{m}_*^-)\right]^{-1} & [\varnothing] \\ \hdashline [\varnothing] & s_2 \cdot \left[-diag(\mathbf{n}_*^-)\right]^{-1} \end{array}\right].$$

For the simple criterion: $\zeta = 1, s_{11} = s_{21} = 1$, whereas for the ASCI LRFD criterion [23], $\zeta = 2, s_{11} = 8/9, s_{21} = 1, s_{12} = 1, s_{22} = 1/2$.
The Lagrange multipliers of the optimum solution of (29) provide the various $\Delta\lambda_i$.

The numerical strategy, presented in Section 4, may now be modified to take into account the moment/axial force interaction. So, starting with $\gamma = 0$ and $k = 1$:

1. Adopt a "fictitious' small initial value for $\Delta\gamma_k = \rho$.
2. Solve the QP problem (29), and obtain a "fictitious" set of increments of hyper-static forces $\Delta\tilde{\mathbf{p}}$ and, using the Lagrange multipliers $\Delta\tilde{\lambda}_i$ of the optimal solution, a set of "fictitious" increments of the generalized plastic displacements $\Delta\tilde{\mathbf{q}}^{pl}$. The QP algorithm [22] is used.
3. Make a first correction to the fictitious set of hyperstatic forces $\Delta\tilde{\mathbf{p}}$ and the various $\Delta\tilde{\lambda}_i$. Also, use (28) to evaluate a set of fictitious $\Delta\mathbf{q}'^{pl}$:
$$\Delta\mathbf{p}' = \frac{1}{\rho} \cdot \Delta\tilde{\mathbf{p}}$$
and
$$\Delta\boldsymbol{\lambda}' = \frac{1}{\rho} \cdot \Delta\tilde{\boldsymbol{\lambda}} \rightarrow \Delta\mathbf{q}_i'^{pl} = \Delta\lambda_i' \cdot \begin{Bmatrix} s_1/m_{*i} \\ s_2/n_{*i} \end{Bmatrix}. \tag{30}$$
4. Evaluate "fictitious" increments of bending and axial forces using (27):
$$\Delta\mathbf{Q}' = \bar{\mathbf{B}} \cdot \Delta\mathbf{p}' + \bar{\mathbf{B}}_o \cdot \mathbf{r}_p \tag{31}$$
and establish the search direction $\Delta\mathbf{Q}_i'$, for each cross section, to determine its next possible plasticization. This occurs at the intersection with one of the yield planes (Fig. 8(a)).
5. Find the correct $\Delta\gamma_k$ as the minimum $\Delta\gamma_{i,k}$ among the non-active constraints that produces a new plasticization at a critical section (Fig. 8(a)):
$$\Delta\gamma_{i,k} = \frac{(\alpha_i \cdot n_{i,k-1} + \beta_i) - m_{i,k-1}}{\Delta m_i' - \alpha_i \cdot \Delta n_i'} \tag{32}$$
for $i = 1, 2, \ldots, N_c$, where N_c is the total number of critical sections. Note that parameters (α_i, β_i) in the above relation may be evaluated using Eq. (22):
$$\alpha_i = -\frac{s_2}{s_1} \cdot \frac{m_{*,i}}{n_{*,i}} \quad \text{and} \quad \beta_i = \frac{m_{*,i}}{s_1}.$$

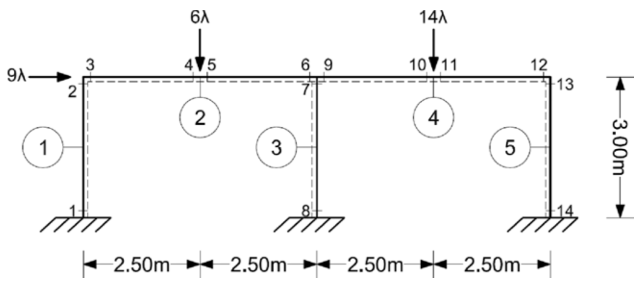

Member	I (m^4)	A (m^2)	M_p (kNm)
1	0.000010	0.003	45.0
2	0.000040	0.004	78.0
3	0.000005	0.002	17.5
4	0.000040	0.004	78.0
5	0.000010	0.003	45.0

Fig. 12. Structure's geometry; members' & critical sections' numbering; mechanical properties; external load pattern.

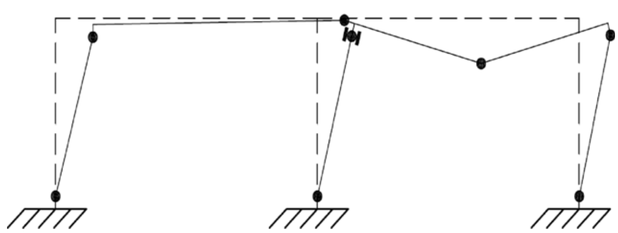

Fig. 13. Collapse mechanism.

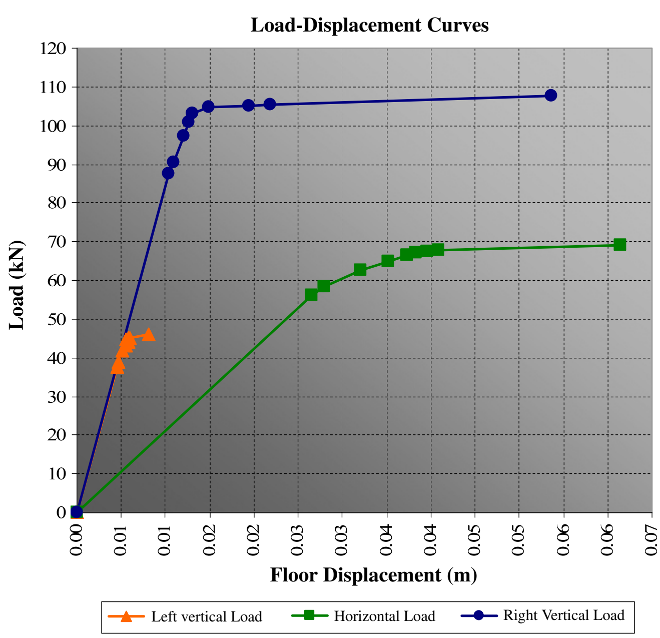

Fig. 14. Load vs. corresponding displacement bearing capacity curves.

For each critical section, $\Delta\gamma_{i,k}$ is the minimum positive among all numbers one would get using (32) for each of the four quadrants of the failure criteria.

6. Find the increments of the bending moments, axial forces and plastic displacements as:

$$\begin{aligned}\Delta\mathbf{m} &= \Delta\gamma_k \cdot \Delta\mathbf{m}',\\ \Delta\mathbf{n} &= \Delta\gamma_k \cdot \Delta\mathbf{n}'\end{aligned} \quad \text{and} \quad \Delta\mathbf{q}^{pl} = \Delta\gamma_k \cdot \Delta\mathbf{q}'^{pl}. \tag{33}$$

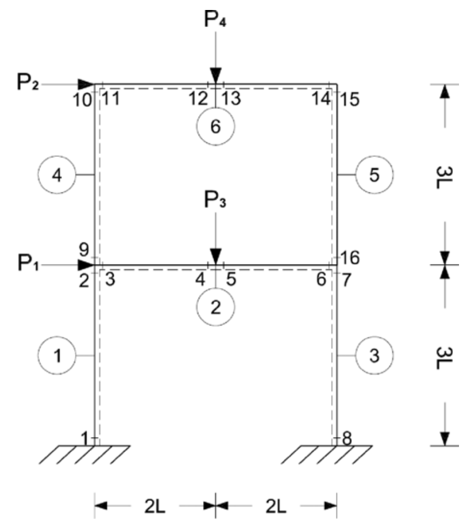

Member Numbers →	1,2,3	4,5,6
I (m^4)	5.10E-05	2.04E-05
E (kN/m^2)	2.10E+08	
σ_y (kN/m^2)	2.20E+05	
M_p (kN·m)	162.0	81.0

Fig. 15. Frame's geometry, loading, member & critical section numbering; mechanical properties.

7. Update the load factor and the various static and kinematic variables:

$$\begin{aligned}
&\gamma_k = \gamma_{k-1} + \Delta\gamma_k\\
&\left.\begin{aligned}\mathbf{m}_k &= \mathbf{m}_{k-1} + \Delta\mathbf{m}\\ \mathbf{n}_k &= \mathbf{n}_{k-1} + \Delta\mathbf{n}\end{aligned}\right] \rightarrow \mathbf{Q}_k\\
&\left.\begin{aligned}\boldsymbol{\theta}_k^{el} &= \mathbf{F}_m \cdot \mathbf{m}_k\\ \boldsymbol{\delta}_k^{el} &= \mathbf{F}_n \cdot \mathbf{n}_k\end{aligned}\right] \rightarrow \mathbf{q}_k^{el} = \bar{\mathbf{F}} \cdot \mathbf{Q}_k\\
&\mathbf{q}_k^{pl} = \mathbf{q}_{k-1}^{pl} + \Delta\mathbf{q}^{pl}\\
&\mathbf{q}_k = \mathbf{q}_k^{el} + \mathbf{q}_k^{pl}.
\end{aligned} \tag{34}$$

The displacements at the loaded points may be found using SKD

$$\mathbf{u}_k = \bar{\mathbf{B}}_0^T \cdot \mathbf{q}_k. \tag{35}$$

8. Return to step 1 and repeat the process for $k = k + 1$, until either
   (a) no solution of the QP may be found, meaning a collapse state has been reached and γ_k is the limit load factor, *or*
   (b) if we have a prescribed loading case and (a) has not occurred, the process stops if $|\gamma_k - \|P_L\|| \leq \rho$, meaning we have reached the end of the current branch.

Once again, the algorithm automatically detects any further plasticization of an already plasticized critical section (point A on Fig. 8(b) and (c) — equivalent to the movement along the directions (1) on the yield plane(s)) or local unloading phenomena (direction (2)), based on whether the corresponding Lagrange multiplier of the active constraint is positive or zero, respectively. We should note here, that, only one constraint will be active when a cross section is plasticized. Even when further plasticization continues along a neighbouring constraint (Fig. 8(c)), the previously active constraint becomes inactive; the neighbouring constraint will be now the only active constraint which gives rise to plastic deformations' increments. The only case where two neighbouring constraints might be simultaneously activated is when the search direction (Fig. 8(a)) meets their point of intersection; two nonzero $\Delta\lambda_i$ now appear for the same cross section. The plastic deformation

Table 1
Bending moment distribution for each analysis step (units: kN, m).

Member	Section	1st	2nd	3rd	4th	5th	6th	7th	8th	9th
1	1	−29.53865	−31.26824	−36.14765	−39.64353	−42.10589	−43.49379	−45.00000	−45.00000	−45.00000
	2	22.01398	23.40427	27.29530	30.10161	32.04830	33.37780	34.50878	35.11547	45.00000
2	3	22.01398	23.40427	27.29530	30.10161	32.04830	33.37780	34.50878	35.11547	45.00000
	4	27.80468	28.73818	31.24522	32.82406	34.01334	33.74192	34.60057	35.00316	41.14113
	5	27.80468	28.73818	31.24522	32.82406	34.01334	33.74192	34.60057	35.00316	41.14113
	6	−60.18756	−62.96819	−69.00010	−72.64524	−74.66283	−78.00000	−78.00000	−78.00000	−78.00000
3	7	−14.63945	−15.43390	−16.60849	−17.50000	−17.50000	−17.41926	−16.05116	−15.58804	−10.00806
	8	16.58555	17.50000	17.50000	17.50000	17.50000	17.50000	17.28631	17.50000	17.50000
4	9	−45.54811	−47.53430	−52.39161	−55.14524	−57.16283	−60.58074	−61.94884	−62.41196	−67.99194
	10	64.13938	66.94652	72.86532	76.15108	78.00000	78.00000	78.00000	78.00000	78.00000
	11	64.13938	66.94652	72.86532	76.15108	78.00000	78.00000	78.00000	78.00000	78.00000
	12	−45.00000	−45.00000	−45.00000	−45.00000	−45.00000	−45.00000	−45.00000	−45.00000	−45.00000
5	13	−45.00000	−45.00000	−45.00000	−45.00000	−45.00000	−45.00000	−45.00000	−45.00000	−45.00000
	14	41.03166	42.06610	45.00000	45.00000	45.00000	45.00000	45.00000	45.00000	45.00000

Table 2
Plasticization/local unstressing sequence & plastic rotations for each analysis step (units: rad).

Member	Section	1st	2nd	3rd	4th	5th	6th	7th	8th	9th
1	1	–	–	–	–	–	–	•	−0.00057	−0.00977
	2	–	–	–	–	–	–	–	–	•
2	3	–	–	–	–	–	–	–	–	–
	4	–	–	–	–	–	–	–	–	–
	5	–	–	–	–	–	–	–	–	–
	6	–	–	–	–	–	•	−0.00180	−0.00285	−0.01620
3	7	–	–	–	•	−0.00068	*−0.00068*	*−0.00068*	*−0.00068*	*−0.00068*
	8	–	•	0.00196	0.00338	0.00409	0.00439	*0.00439*	•	0.00858
4	9	–	–	–	–	–	–	–	–	–
	10	–	–	–	–	•	0.00169	0.00533	0.00738	0.03310
	11	–	–	–	–	–	–	–	–	–
	12	–	–	–	–	–	–	–	–	–
5	13	•	−0.00111	−0.00396	−0.00538	−0.00631	−0.00742	−0.00965	−0.01110	−0.03060
	14	–	–	•	0.00100	0.00171	0.00205	0.00250	0.00292	0.00977

Table 3
Loading cycle (units: kN).

Loading cycle point	P_1	P_2	P_3	P_4
1	86.0	43.0	258.0	129.0
2	0.0	0.0	0.0	0.0
3	86.0	43.0	0.0	0.0
4	0.0	0.0	0.0	0.0

increments for this cross section will now be evaluated as the composition of two vectors [1], one for each yield plane, that are determined using (28).

The procedures described are stable, robust and computationally efficient. The flexibility matrix is established at the first step and is decomposed only once. There is no need of any further reformulation or re-decomposition whenever a new plastic hinge or any local unloading might take place. The QP program is solved only once at each incremental step and the step length that marks the next plasticization is automatically determined without having to perform unnecessary intermediate elastic steps of fixed length as would be the case in any of the existing computer packages that are based on the direct stiffness method.

The parameter "ρ" is a pure number, and does not depend on the adopted units. Although the procedure is stable for any "ρ", for good accuracy reasons, its' value is chosen so as to be able to capture all possible plasticization events, no matter how close they are to each other.

6. Numerical examples

A computer program that follows the above described procedure was written in FORTRAN. The IMSL routine DQPROG [24] was included to implement the algorithm of [22]. Overall, a value of $\rho = 10^{-3}$ to 10^{-4} has proved sufficient for all examples presented herein.

Five examples of application are used to demonstrate the versatility of the proposed procedure. The first four examples assume a pure bending behaviour. All kinds of inelastic analyses like monotonic loading, piecewise proportional loading, cyclic loading and pushover analysis are tested. In the fifth example moment/axial force interaction is considered. Both the simple and the AISC LFRD criteria have been applied.

Nonholonomic behaviour is assumed throughout as it was shown above that it may easily be accounted for and it represents a more realistic behaviour, despite the fact that most commercial packages do not have or have improper facilities to accommodate it (e.g. SAP2000 [16]). The computational efficiency of the approach is demonstrated on a problem of a relatively large scale.

6.1. Simple frame under prescribed loading

The frame of Fig. 9 is analyzed as a first example. The bending stiffness, as well as the bending plastic capacity of the various members is shown in the same figure.

This example was solved by hand in Smith and Munro [25]. It is a prescribed loading case, with the horizontal load being applied first up to the level of 50 kN, then the vertical load is applied up to the level of 160 kN with the horizontal load being kept constant, and finally the two loads are proportionally varied, the horizontal being decreased to 20 kN, whereas the vertical is increased to 180 kN. The loading scenario may be seen in Fig. 10. All the important events are shown in the same figure. It may be seen that a plastic hinge

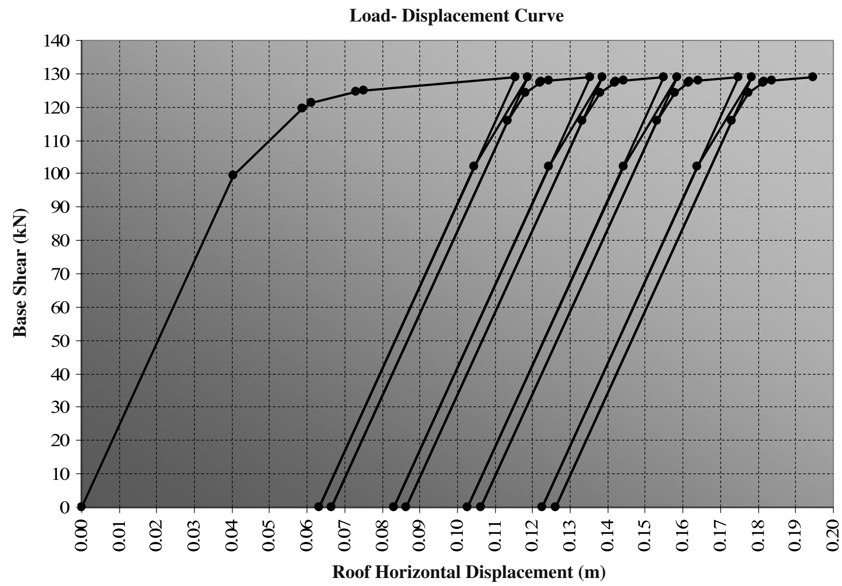

Fig. 16. Base shear vs. roof horizontal displacement curve.

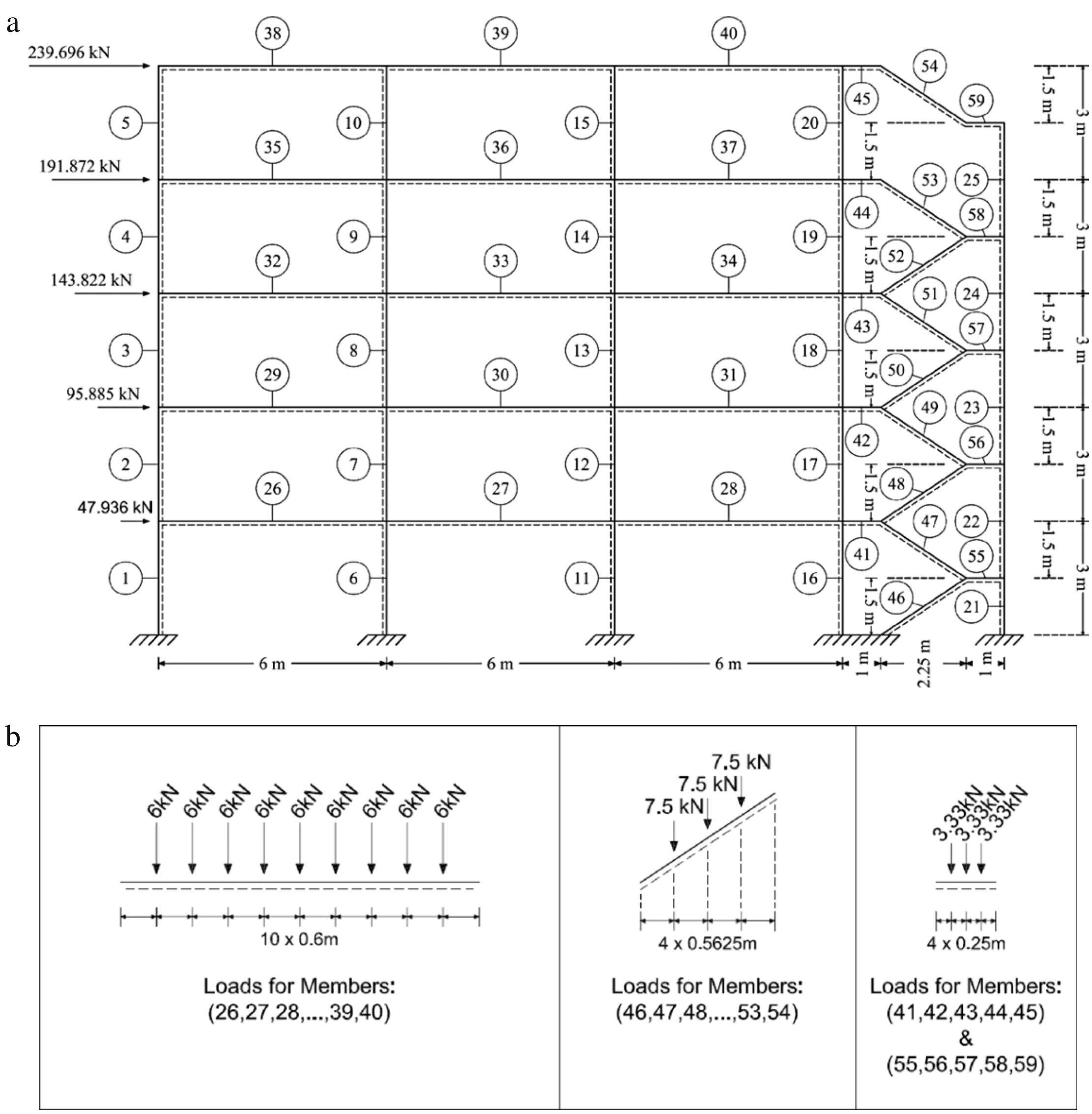

Fig. 17. (a) Structure's geometry, seismic loads, member numbering. (b) Uniform dead load on beams.

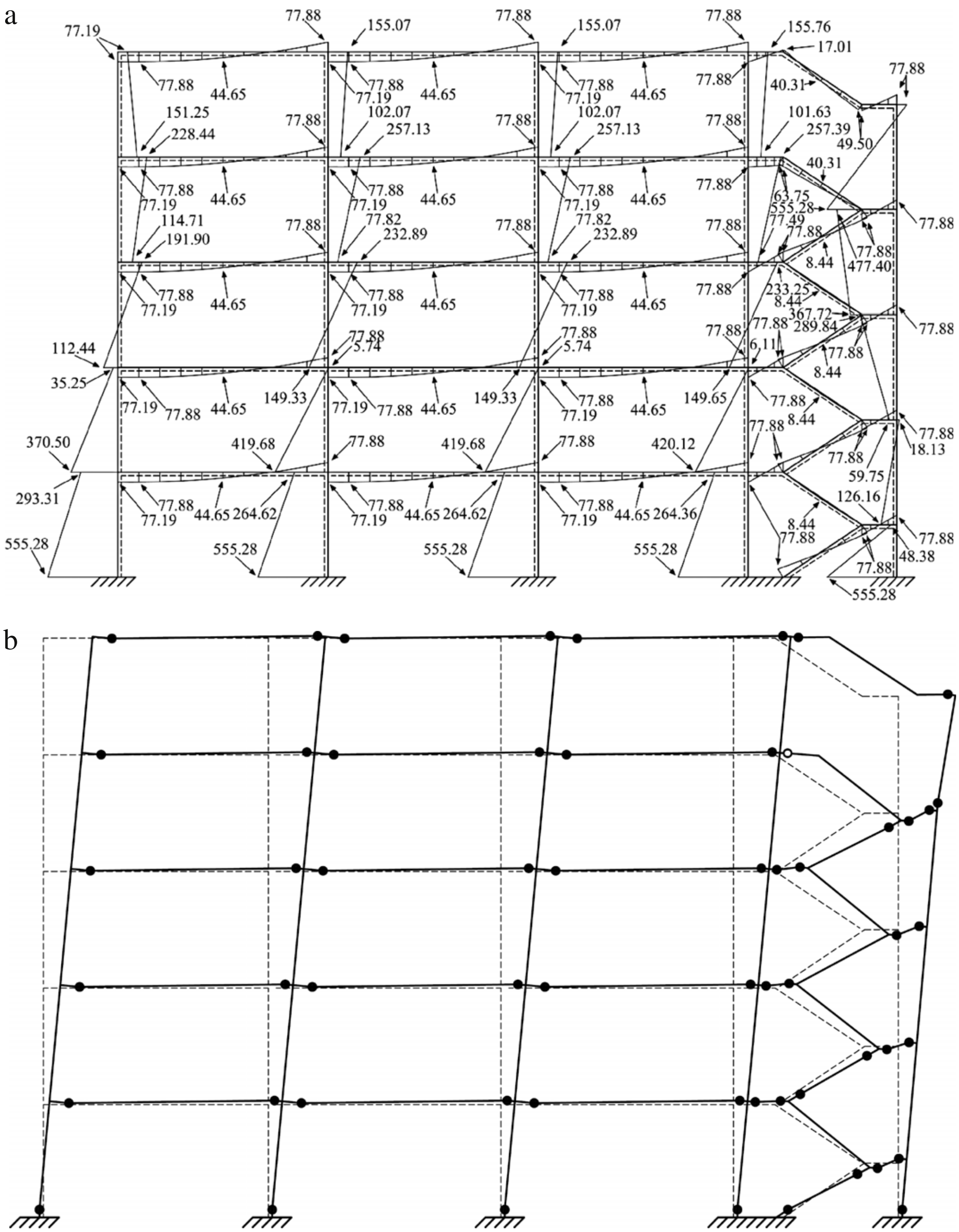

Fig. 18. (a) Bending moment diagram on collapse (units: kN m). (b) Collapse mechanism.

forms at section 2 first. Then, it unloads at the third step resulting to a remaining $\theta_{pl}^{(2)} = +3.33\text{E}-02$ rad, while another hinge forms at section 7. At the fifth step, this section unloads resulting to a remaining $\theta_{pl}^{(7)} = -1.33\text{E}-01$ rad, while another hinge forms at section 4, leaving a $\theta_{pl}^{(4)} = +8.33\text{E}-03$ rad, at the end of the sixth step (see Fig. 10).

The evolution of the bending moments is shown in Fig. 10. Results coincide with the ones obtained in [25].

The load–deflection curves for the two loads and the corresponding displacements are shown in Fig. 11.

6.2. Limit analysis of a two-bay frame

The second example of application is the limit analysis of a two bay frame shown in Fig. 12, with λ being the load factor. Despite the fact that the loading is monotonic, plastic unstressing occurs. This example has been solved in the work of Franchi and Cohn [7], using a rather complex algorithm.

The evolution of the bending moments may be seen in Table 1. The sequence of plasticization/local unloading events, as well as the plastic rotations' values, may be seen in Table 2, where a bullet (•) symbolizes the activation of the corresponding plastic hinge at the current step. Local unstressing of a previously activated hinge is denoted with italics. As it can be seen from Table 2, the cross section 7 starts unloading at the sixth step and continues unstressing till the end. On the other hand, the cross section 8 unloads at the seventh step, but reloads at the next step and remains plasticized through the end. The collapse mechanism appears in Fig. 13 and the bending moment distribution at the state of collapse in the last column of Table 1.

Finally the various load vs. corresponding deflection curves for the three loads appear in Fig. 14.

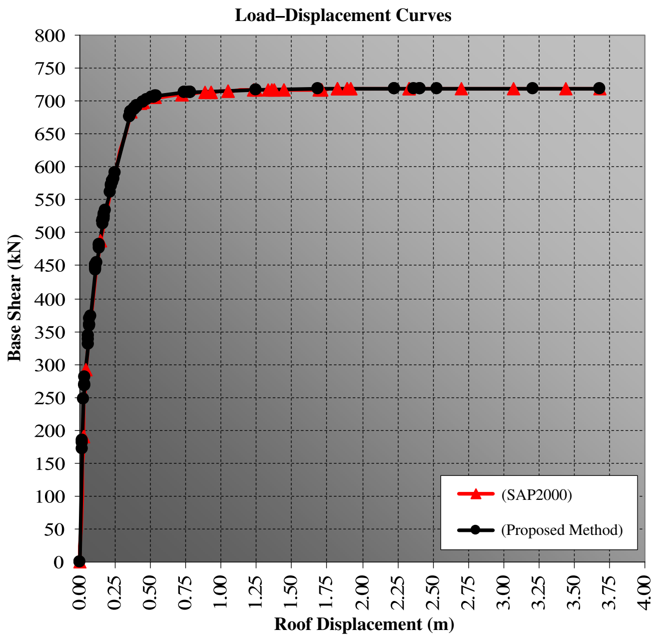

Fig. 19. Static pushover analyses curves.

6.3. Two-storey frame under cyclic loading

Cyclic loading, which is a special case of prescribed loading, is chosen as the next application. The example consists of a two-storey frame that is subjected to horizontal and vertical loads (Fig. 15). The mechanical properties of the members can be seen in Fig. 15. Results are presented for $L = 1$ m.

The loading cycle consists of applying both horizontal and vertical loads at first, then unloading to zero, then applying the horizontal loads only, and unloading to zero again. The maximum values that the loads reach inside the cycle (Table 3) have been selected so that they are above their corresponding shakedown values $\mathbf{P}_{sh} = \{P_1, P_2, P_3, P_4\}_{sh} = \{82.296, 41.148, 246.888, 123.444\}$ (units: kN) that have been estimated by Nguyen and Morelle [26]. The bending moment diagram that develops inside a cycle may be seen in Table 4. From these results one realizes the development of plastic hinges at sections 4, 6, 8, 11 and 14 (see Fig. 15) in the first part of the loading cycle which all eventually unload in the second part, whereas a new plastic hinge opens at section 1 at the third part of the cycle. These hinges form an incremental collapse mechanism. Also, in the same table, one may see the values of the plastic rotations at the end of the first cycle, as well as their increments over the second cycle. These increments become constant over the third and subsequent cycles leading to incremental collapse. The base shear (*loads* $P_1 + P_2$) vs. roof horizontal displacement curve for the first four loading cycles may be seen in Fig. 16. Despite the fact of the formation of plastic hinges very close to each other, the procedure with $\rho = 0.0001$ is capable of capturing all of them, thus proving the method's effectiveness once more.

6.4. Pushover analysis of a multi-storey frame

This example is a static pushover analysis on a five-storey plane frame, and is presented here to demonstrate the algorithm's efficiency on relatively large-scale problems of common engineering practice.

In Fig. 17(a) the structure's geometry and member numbering may be seen. The assumed material is S220. In order to achieve a strong column-weak beam collapse mechanism, sections HEM260

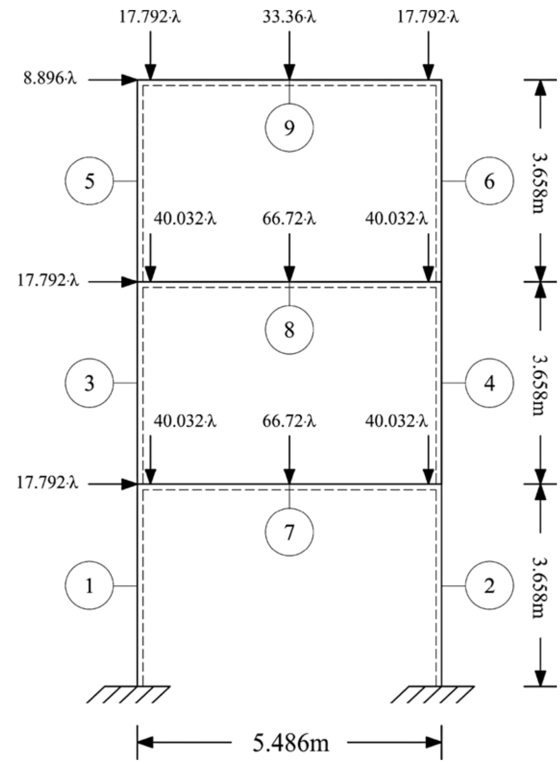

Member	Section
1	W 8x28
2	
3	W 6x25
4	
5	W 6x20
6	
7	W 12x27
8	
9	W 10x21

Fig. 20. Frame geometry, member numbering and initial loading coefficients. (units: kN).

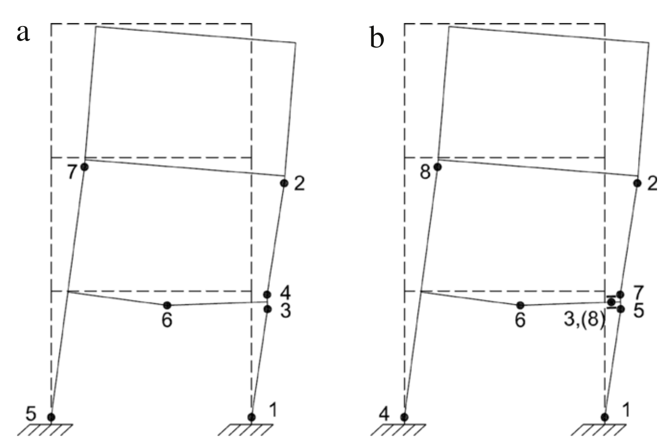

Fig. 21. Collapse mechanism and plasticization/local unstressing sequence for each criterion: (a) $(m/m_*) + (n/n_*) = 1$. (b) AISC LFRD.

(*with EI* $= 65751.0$ kN m^2, $M_p = 555.28$ kN m) were assigned to the columns, and to all beams (including the inclined members) sections HEB160 (*with EI* $= 5233.2$ kN m^2, $M_p = 77.88$ kN m). The

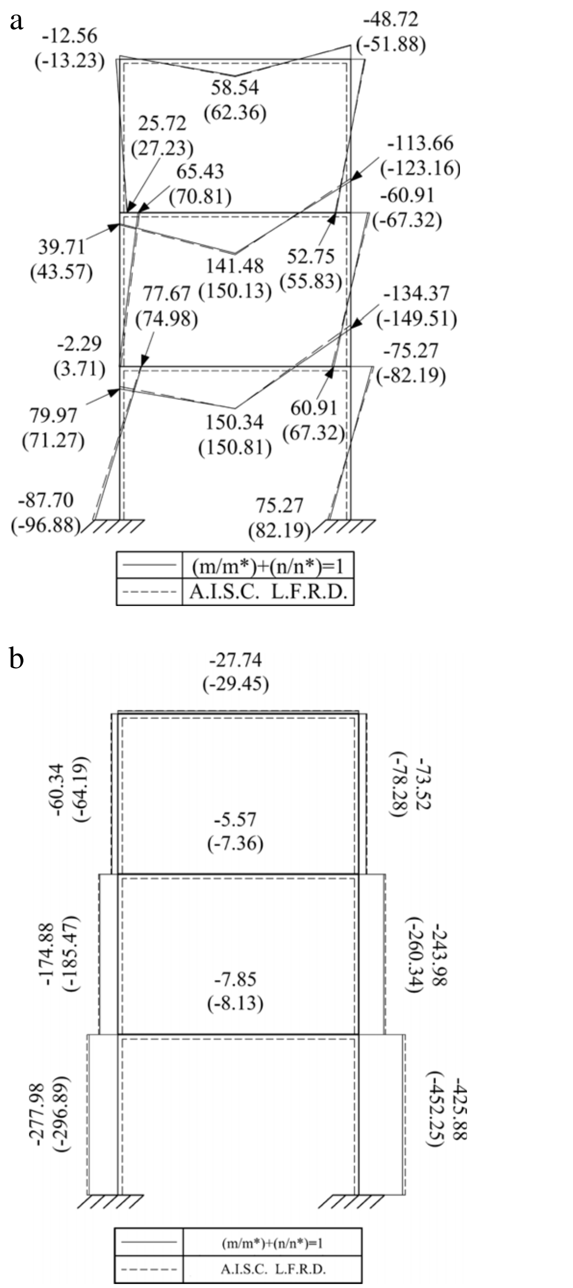

Fig. 22. (a) Bending moments distribution on collapse. (units: kN m). (b) Axial forces distribution on collapse. (units: kN).

earthquake loads were computed according to the EAK 2000 [27] having linear distribution along the height and are applied at the level of each floor (Fig. 17(a)), while the dead load for the various types of beams of the structure may be seen in Fig. 17(b).

For the sake of checking computational efficiency in terms of the number of constraints, and in order to approximate the exact locations of plastic hinges along the beams more accurately, distributed loads are modeled as a finite set of quite close and equally positioned, statically equivalent point loads. Two types of beam vertical loading were appointed; beam members 26 to 40 & 46 to 54 were subjected to point loads equivalent to a uniform loading of magnitude $q = 9$ kN/m, while members 41 to 45 & 55 to 59 to point loads equivalent to 10 kN/m (see Fig. 17(b)). Due to this simulation, the structure ends up having a total of 502 critical sections. Since for each critical section we have two inequality constraints, this yields a total of 1004 constraints.

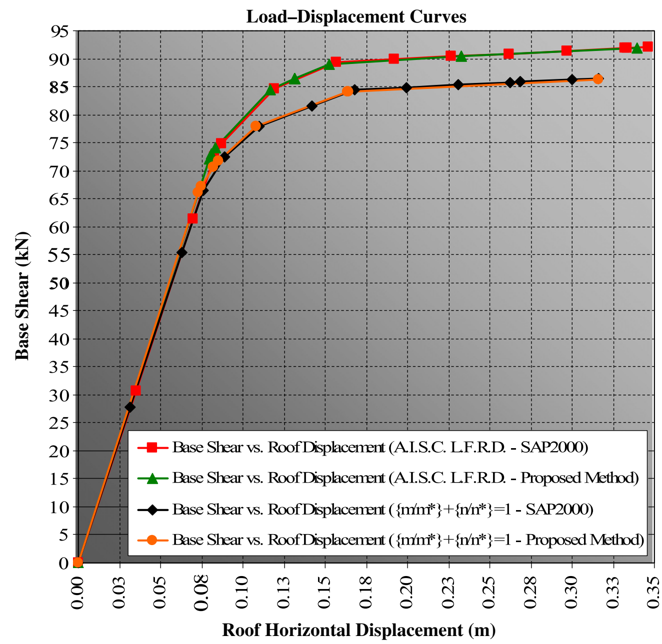

Fig. 23. Horizontal loads vs. corresponding horizontal displacement curves.

Pushover analysis with the proposed method is performed in the form of a prescribed loading. At first, only the vertical (*dead*) loads are applied; then the earthquake loads are added to the existing load/stress state and are monotonically increased until collapse occurs.

The best accuracy was acquired by using $\rho = 0.0001$. Plasticization started from the small horizontal beams that are connected to the exterior column on the right. In the course of the analysis, the characteristic of a numerical nonholonomic analysis, i.e. the formation of hinges that were loaded, unloaded and reloaded, or permanently unloaded, often appeared.

Results show that the plastic hinges develop close to or exactly at the members' ends. The values of the earthquake loads that brought the structure to collapse are shown in Fig. 17(a). The bending moments' diagram at the state of collapse, for the whole structure, appears in Fig. 18(a). The hinges in the final collapse mechanism may be seen in Fig. 18(b).

The results of the proposed method were compared to those of a widely used commercial package (SAP2000 [16]), that uses the direct stiffness method. In order to match the total number of the critical sections, 256 finite elements were used to model the problem examined. As one may see from Fig. 19, the base shear forces versus the roof displacement curves for both the analyses are almost identical. The collapse mechanism was also identical.

The time required by SAP2000 to solve the problem, with the default analyses options, may be seen in Table 5. Note that, only for inverting the stiffness matrix, 13.31 s were needed, while the total time for calculations was 22.55 s. On the other hand, using the proposed method, solution was acquired within only 3.78 s. Computations were performed on an Intel Core2 Duo T8100 microprocessor (2.1 GHz), using only one of the CPU's cores.

6.5. Limit analysis of a three-storey frame with $\{m, n\}$ interaction

The fifth example shows the application of the proposed algorithm to a 3-storey frame when considering (m, n) interaction. This example was first presented as a limit analysis problem by Cohn & Rafay [28].

The structure's geometry, loading, member numbering and section types for each member, may be seen in Fig. 20; the three

Table 4
Bending moments values inside a cycle; changes of plastic rotations over loading cycles (units: kN, m).

Member	Section	Bending moments for every loading cycle point				θ_{pl} at the end of the 1st cycle	$\Delta\theta_{pl}$ at the end of the 2nd cycle	$\Delta\theta_{pl}$ at the end of each subsequent cycle
		1st	2nd	3rd	4th			
1	1	−156.000	−67.108	−162.000	−42.106	–	−3.300E−03	−3.300E−03
	2	−17.357	−28.961	44.665	−28.942	–	–	–
2	3	−30.000	−28.397	77.704	−26.442	–	–	–
	4	162.000	9.749	7.152	7.152	2.800E−02	6.600E−03	6.600E−03
	5	162.000	9.749	7.152	7.152	–	–	–
	6	−162.000	47.895	−63.401	40.745	−3.090E−02	−6.600E−03	−6.650E−03
3	7	−86.357	49.252	−34.102	39.504	–	–	–
	8	162.000	11.105	146.233	26.339	4.280E−03	3.300E−03	3.305E−03
4	9	12.643	−0.564	−33.039	−2.500	–	–	–
	10	−15.000	1.330	36.000	2.039	–	–	–
5	11	−81.000	3.252	−30.662	3.298	−2.780E−02	−6.600E−03	−6.650E−03
	12	75.643	1.357	29.299	−1.241	–	–	–
6	13	−15.000	1.330	36.000	2.039	–	–	–
	14	81.000	2.291	2.669	2.669	2.450E−02	6.600E−03	6.600E−03
	15	81.000	2.291	2.669	2.669	–	–	–
	16	−81.000	3.252	−30.662	3.298	–	–	–

Table 5
SAP2000 v.14.0.0 computational time table.

Time for initializing analysis	= 0.10
Time for controlling analysis	= 3.59
Time for forming stiffness matrix	= 0.35
Time for solving stiffness matrix	= 13.31
Time for calculating displacements	= 4.11
Time for determining events	= 0.15
Time for updating state	= 0.94
Total time for this analysis	= 22.55

decimal point accuracy is due to conversion from Imperial to S.I. units.

Two types of analysis were performed; one based on the simple criterion, as in [28], and one based on the AISC LFRD criterion [23]. The value $\rho = 0.001$ was used for the fictitious load increment in both cases.

For the simple criterion case, the limit load factor was found $\lambda_c = 1.94177$, almost identical with the one given in [28] ($\lambda_c = 1.952$), whereas for the AISC LFRD criterion case, the limit load factor was $\lambda_c = 2.06649$.

The collapse mechanism and the plasticization sequence for the two criteria are shown in Fig. 21(a) and (b), where the numbers correspond to the analysis step in which the event takes place. One may notice the difference in the plasticization sequence between the two cases. In the AISC LFRD case (see Fig. 21(b)), the critical section at the right end of member 7 that was plasticized in step 3 is unstressed in step 8, while – in the same step – a new plastic hinge forms at the upper end of member 3.

The bending moments' and axial forces' diagrams on the state of collapse for each criterion case are shown in Fig. 22(a) and (b), with the values inside the parentheses corresponding to the AISC LFRD criterion analysis results.

In Fig. 23, one may see the base shear vs. roof horizontal displacement curves, for both bending moment and axial force interaction criteria.

The same example was solved using SAP2000 [16], yielding identical results (Fig. 23). For the simple criterion, 2.70 s were required in total, while 1.86 s were required for solving only the stiffness matrix. On the other hand, using the proposed method, the total computational time was only 0.047 s. For the AISC LFRD, 3.17 s were required in total, while 2.19 s were required for solving only the stiffness matrix. On the other hand, using the proposed method, the total computational time was only 0.062 s. Computations were performed on an Intel Core2 Duo T8100 microprocessor (2.1 GHz), using only one of the CPU's cores.

7. Concluding remarks

A force based numerical procedure that deals with the nonholonomic elastoplastic analysis of frames has been presented. A relatively simple algorithm is used to select the hyperstatic forces which are the basic unknowns.

The method is developed within the framework of mathematical programming. It is formulated as an incremental PQP problem. The PQP problem is converted to a QP problem through the use of a fictitious loading step. In this way, a good QP algorithm may be used for the solution. No extra numerical care needs to be taken, since plastic unstressing, in a stepwise holonomic way, is naturally accommodated in the procedure.

The method was first formulated for frame structures of pure bending behaviour. It was then extended to cater for axial force effects also. Examples of application for both types of behaviour have been presented.

The procedure turned out to be accurate, stable and computationally superior as compared to the direct stiffness method that is almost exclusively used. It is therefore believed that this could enhance the use of mathematical programming methods towards the numerical solution of elastoplastic problems.

The proposed method may be extended to 3D structures. Material hardening may also be included.

References

[1] Maier G. A quadratic programming approach for certain classes of non linear structural problems. Meccanica 1968;3:121–30.
[2] Maier G. Quadratic programming and theory of elastic–perfectly plastic structures. Meccanica 1968;3:265–73.
[3] Maier G. A matrix structural theory of piecewise linear elastoplasticity with interacting yield planes. Meccanica 1970;5:54–66.
[4] De Donato O, Maier G. Historical deformation analysis of elastoplastic structures as a parametric linear complementarity problem. Meccanica 1976; 11:166–71.
[5] Smith DL. The Wolfe–Markowitz algorithm for nonholonomic elastoplastic analysis. Eng Struct 1978;1:8–16.
[6] Maier G, Giacomini S, Paterlini F. Combined elastoplastic and limit analysis via restricted basis linear programming. Comput Methods Appl Mech Engrg 1979; 19:21–48.
[7] Franchi A, Cohn MZ. Computer analysis of elastic–plastic structures. Comput Methods Appl Mech Engrg 1980;21:271–94.
[8] Kaneko I. Complete solutions for a class of elastic–plastic structures. Comp Meth Appl Mech Engrg 1980;21:193–209.

[9] Wakefield RR, Tin-Loi F. Large scale nonholonomic elastoplastic analysis using a linear complementarity formulation. Comp Meth Appl Mech Engrg 1990;84: 229–42.
[10] Coccheti G, Maier G. Elastic–plastic and limit-state analyses of frames with softening plastic-hinge models by mathematical programming. Int J Solids Struct 2003;40:7219–44.
[11] Tangaramvong S, Tin-Loi F. Limit analysis of strain softening steel frames under pure bending. J Const Steel Res 2007;63:1151–9.
[12] Tangaramvong S, Tin-Loi F. A complementarity approach for elastoplastic analysis of strain softening frames under combined bending and axial force. Eng Struct 2007;29:742–53.
[13] Marin-Artieda CC, Dargush GF. Approximate limit load evaluation of structural frames using linear elastic analysis. Eng Struct 2007;29:296–304.
[14] Barrera O, Cocks ACF, Ponter ARS. Evaluation of the convergent properties of the Linear Matching Method for computing the collapse of structural components. Eur J Mech A Solids 2009;28:655–67.
[15] Tin-Loi F, Wong MB. Nonholonomic computer analysis of elastoplastic frames. Comput Methods Appl Mech Engrg 1989;72:351–64.
[16] SAP2000, v14.0.0. User's manual. CSI Inc. 2009.
[17] Pereira NZ, Borges LA, Hecke MB. A force method for elastic–plastic analysis of frames by quadratic optimization. Int J Solids Struct 1988;24:211–30.
[18] Damkilde L, Høyer O. An efficient implementation of limit state calculations based on lower-bound solutions. Comput Struct 1994;6:953–62.
[19] Spillers WR. Application of topology in structural analysis. J Struct Div ASCE 1963;89:301–13.
[20] Spiliopoulos KV. On the automation of the force method in the optimal plastic design of frames. Comput Methods Appl Mech Engrg 1997;141:141–56.
[21] Spiliopoulos KV. A fully automatic force method for the optimal shakedown design of frames. J Comput Mech 1999;23:299–307.
[22] Goldfarb D, Idnani A. A numerically stable dual method for solving strictly convex quadratic programs. Math Program 1983;27:1–33.
[23] Load and resistance factor design specification for structural steel buildings. 2nd ed. Chicago: American Institute of Steel Construction; 1993.
[24] IMSL Fortran Library V 6.0. 2007.
[25] Smith DL, Munro J. On uniqueness in elastoplastic analysis of frames. J Struct Mech 1978;6:85–106.
[26] Nguyen DH, Morelle P. Optimal plastic design and the development of practical software. In: Smith DL, editor. Mathematical programming methods in structural plasticity. CISM courses and lectures, No. 299. 1990. p. 207–29 [Chapter 12].
[27] EAK 2000. Greek Code for earthquake resistant structures. 2000.
[28] Cohn MZ, Rafay T. Collapse load analysis of frames considering axial forces. J Eng Mech ASCE 1974;100(4):773–94; J Eng Mech ASCE 1975;101(4):493–4 [errata].